Environmental Science & Technology LETTERS

pubs.acs.org/journal/estlcu

Letter

Enhanced Wet Deposition of Nitrogen Induced by a Landfalling Typhoon over East Asia: Implications for the Marine Eco-Environment

Ying Zhang, Xingtao Su, Baozhu Ge,* Xiaobin Xu, Qixin Tan, Guanghua Chen, Danhui Xu, Xueshun Chen, Lin Wu, Meng Gao, Xiaole Pan, Jianping Guo, Xuejun Liu, Joshua S. Fu, and Zifa Wang

Cite This: *Environ. Sci. Technol. Lett.* 2022, 9, 1014−1021

Read Online

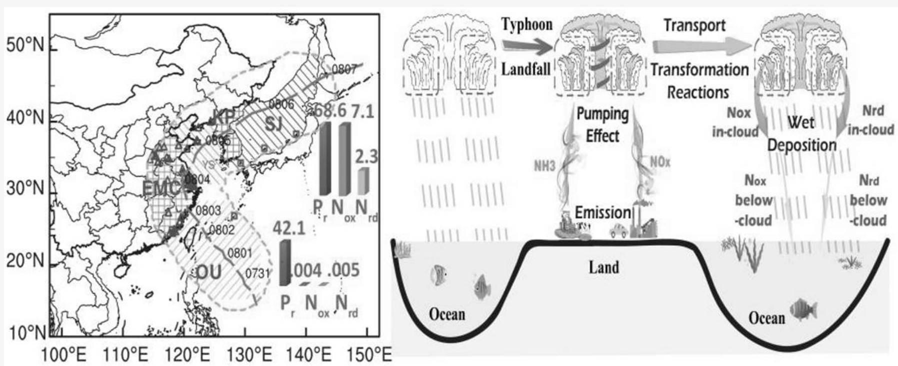

ABSTRACT: Wet deposition of reactive nitrogen (N_r) induced by typhoons has significant eco-environmental impacts on the oceans, especially under the growing frequency of landfalling typhoons in East Asia. However, little is known about the mechanism of how anthropogenic activities influence the ocean ecosystem by interacting with landfalling typhoons. Based on the Nested Air Quality Prediction Modeling System, the N_r wet deposition induced by landfalling typhoon Hagupit 2020 and the ecological response were explored. The N_r wet deposition over both the Yellow Sea and the Sea of Japan after landfall was found to have increased by up to 1000 times that of the prelandfall ocean influenced by the typhoon. This high N_r wet deposition was mainly due to the "pumping effect" mechanism of the typhoon, where strong uplifts of the typhoon rapidly carried surface air pollutants up to high altitudes from the land, following a large wet deposition through long-range transport toward the downwind ocean, finally leading to a high-concentration chlorophyll-a bloom. This study improves our understanding of N_r wet deposition induced by landfalling typhoons and helps in the establishment of effective and active measures and to reveal marine ecology damaged by extremely strong convective weather systems.

KEYWORDS: *reactive nitrogen (N_r), wet deposition, landfalling typhoon, pumping effect, marine ecological response*

■ INTRODUCTION

Atmospheric reactive nitrogen (Nr) (including oxidized N (N_{ox}) and reduced N (N_{rd})) deposition to the ocean is an important nutrient source of marine ecosystems in N-limited regions,[1−4] which is equivalent to or even greater than that of the riverine input[5−8] over ocean areas of East Asia, with considerable effects on productivity, ocean acidification, and emissions of greenhouse gases such as N_2O.[5,9] The emissions of NO_x from China have increased 6-fold from 1980 to 2010[8,10] and reached a peak in 2011 before subsequently declining following stringent emission controls.[11] However, ammonia (NH_3) emissions in East Asia continue to grow,[12,13] which greatly influence the formation of nitrate (NO_3^-) and ammonium (NH_4^+) aerosol. Consequently, the paticulate NO_3^- has not responded effectively to decreasing NO_x emissions,[14,15] which was also confirmed by EANET (Acid Deposition Monitoring Network in East Asia) observations.[16]

The increased anthropogenic Nr emitted from northeast Asian countries to East Asian marginal seas has resulted in an incomparable increase in the N concentration predominantly explained by increased atmospheric deposition,[17] which could lead to a high risk of N pollution and strongly influences the biogeochemical cycles of ecosystems over East Asia. Over

Received: October 18, 2022
Revised: November 19, 2022
Accepted: November 22, 2022
Published: November 30, 2022

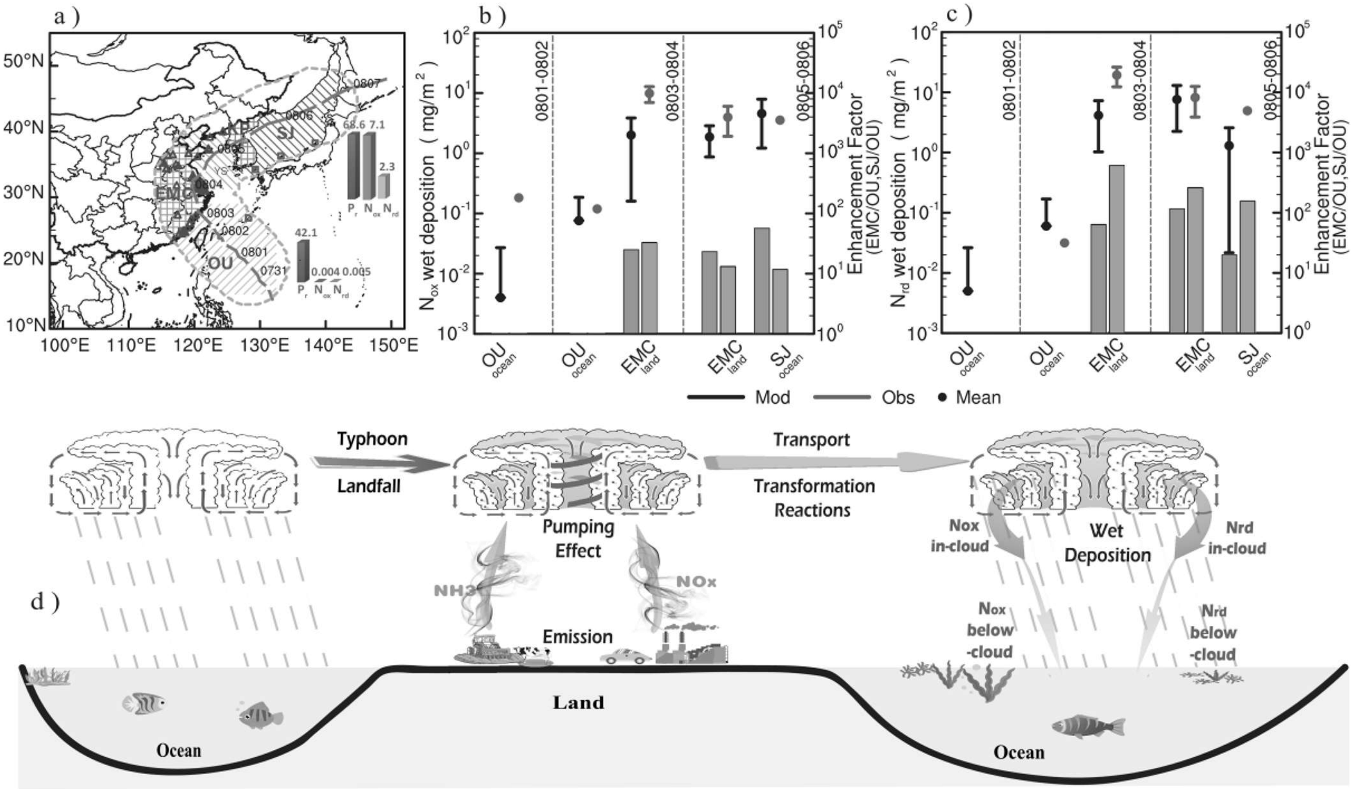

Figure 1. Distribution of the monitoring stations (blue triangles for CNEMC; brown squares for EANET) and the typhoon-affected regions (surrounded by orange short-dashed lines) between 1 and 6 August 2020, as well as the divided regions of interest located in the ocean lying upwind of the Asian continent (OU, pink), Yellow Sea, Bohai Sea, and part of the northern East China Sea (YS, orange), Sea of Japan (SJ, violet), eastern mainland China (EMC, green), and the Korean Peninsula (KP, sky blue). Crosshatching represents land areas, and stripes represent ocean areas. The purple line represents the track of typhoon Hagupit; the histograms represent the averaged accumulated precipitation (blue) and N_{ox} (orange) and N_{rd} (yellow) wet depositions (a). Temporal variations (left axis) of observations (red circles) and simulations (black circles) for the wet depositions of N_{ox} (b), and N_{rd} (c). Whiskers for the observations and models represent one-third of the standard deviation of estimates. Enhancement factor of typhoon (right axis)-induced wet depositions from observations (gray bar) and simulations (red bar), respectively. Schematic diagram of landfalling typhoon-induced wet deposition over East Asian oceans (d). "In-cloud" represents the in-cloud wet deposition, while "below-cloud" is the below-cloud wet deposition.

ocean areas of East Asia, symptoms of eutrophication (including harmful algal blooms, hypoxia, and biodiversity loss) have increased noticeably since the 1970s, which appear to be associated with increasing N concentrations.[18] Meanwhile, anthropogenically induced increases in atmospheric N deposition to the ocean can stimulate marine productivity.[4,19] The annual total N deposition can be converted to new marine productivity of 100−200 mmol C m^{-2} yr^{-1}, which is 1.1%−3.9% of the new productivity in the East China Sea.[5] In addition, the wet deposition of fine-mode NH_4^+ and NO_3^- makes a significant contribution to the total N deposition over East Asian oceans, especially the Yellow Sea (YS) and Sea of Japan (SJ).[8]

Among a variety of processes, cyclones are an important source of N wet deposition, and thus, the characterization of cyclone-related wet deposition is integral to understanding how future extreme weather events will impact marine biogeochemical cycles.[20] Large cyclone-related wet deposition events can make a significant proportion of the typical average annual N deposition within just a few hours,[21] with the typical annual wet deposition accounting for 79% of total N deposition in China's eastern seas.[5] The rapid and large increases in wet deposition during the passage of a cyclone may lead to ecosystems greatly exceeding their critical N loading thresholds for biodiversity risk.[22−24] However, it has not been investigated in detail how typhoons and the surrounding circulations impact the wet deposition over East Asian oceans. Additionally, given the high amount of N deposition affecting the marine environment, it is critical to quantitatively study the influence of landfalling typhoon-induced wet deposition in East Asian oceans and the corresponding underlying mechanisms. Here, we used a regional chemical transport model—the Nested Air Quality Prediction Model System (NAQPMS)[25−27]—to quantify the influence of the increases in N_r deposition on the marine eco-environment and identify the mechanisms of N_r wet deposition induced by landfalling typhoons. The results will provide a basis for further understanding how future extreme weather events may impact marine biogeochemical cycles.[20]

■ MATERIALS AND METHODS

Description and Configuration of NAQPMS. NAQPMS, which is a 3D Eulerian terrain-following air quality model widely used to investigate the wet deposition and wet scavenging of soluble inorganic ions,[27,28] was adopted in this study.[25] The model horizontal domain covers the region of East Asia (15.4°S−58.3° N, 48.5°−160.2° E) on a Lambert conformal map projection, with 182 × 172 grids at a 45-km horizontal resolution. Vertically, the model uses 20 terrain-following layers from the surface to 20 km a.s.l., with the lowest

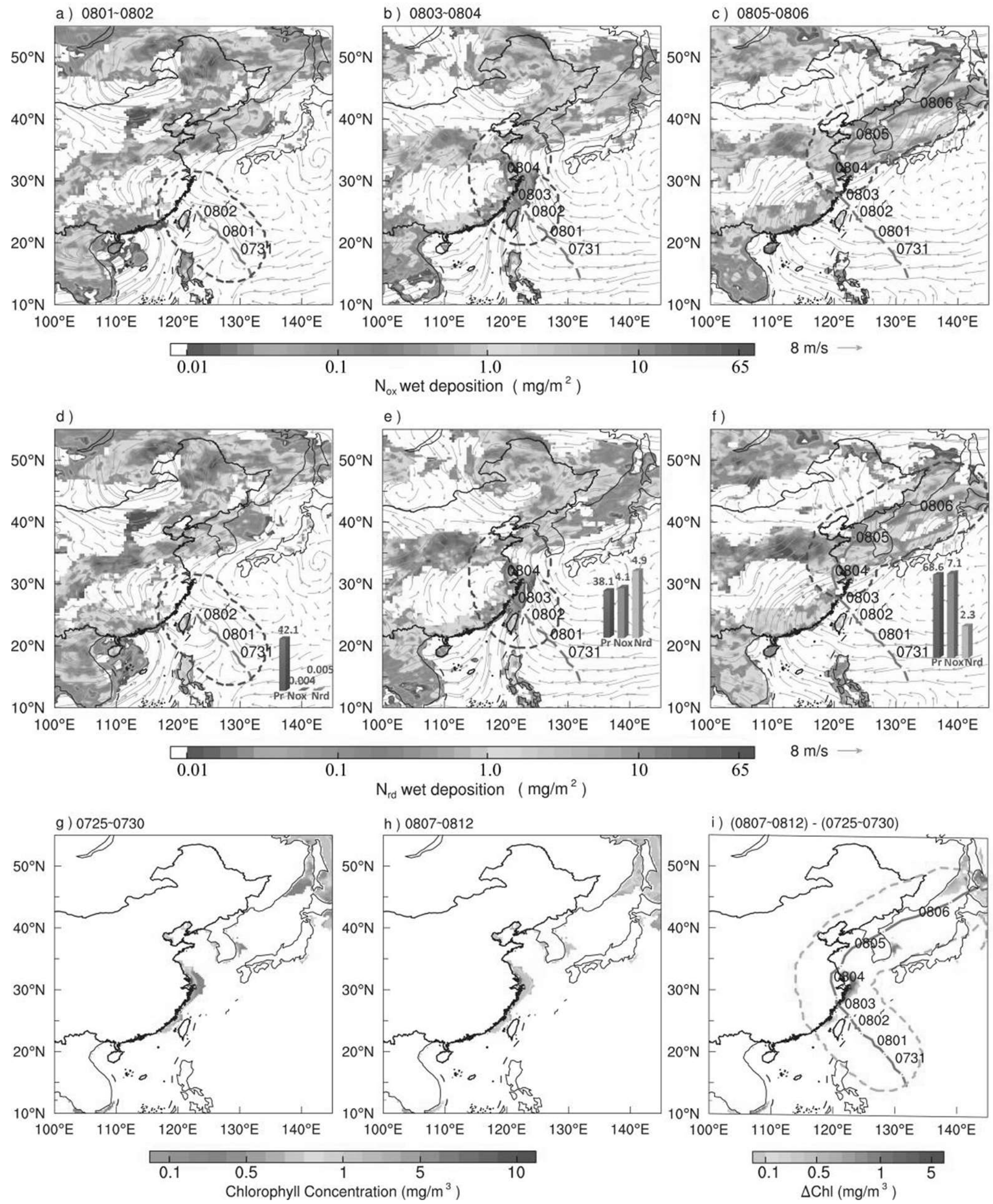

Figure 2. Spatial distributions of N_{ox} (a−c) and N_{rd} (d−f) wet depositions during typhoon Hagupit's prelandfall (a, d; 1−2 August), landfall (b, e; 3−4 August), and postlandfall (re-emerging over the sea; c, f; 5−6 August). The areas surrounded by blue short-dashed lines represent the regions affected by typhoon Hagupit. The purple lines represent their corresponding typhoon tracks from model simulations (a−c) and the Japan Meteorological Agency (d−f) of typhoon Hagupit at 6-h intervals. The histograms represent the averaged accumulated precipitation (blue) and N_{ox} (orange) and N_{rd} (yellow) wet depositions, among the typhoon prelandfall, landfall, and postlandfall stages. Spatial distributions of average chlorophyll-a concentrations in bloom for 6 days before the typhoon's passage as reference (g, 25−30 July) and 6 days after typhoon as ecological response (h, 7−12 August), as well as their corresponding anomalies (i, h, g).

nine layers below 2 km. The global chemistry transport model, MOZART version 2.4, provided initial and lateral boundary conditions for NAQPMS. The anthropogenic emissions inventory entered into the model included the MIX anthropogenic emissions over Asia developed for MICS-Asia Phase III,[29] the biogenic emissions calculated by MEGAN (Model of Emissions of Gases and Aerosols from Nature) version 2.04,[30] and the biomass burning emissions from GFED (Global Fire Emissions Database) version 3.[31] Furthermore, the emissions inventory was updated according to the observational data based on the latitudes and longitudes of the state control sites. Additional descriptions of the model can be found in the Supporting Information (SI) Text S1.

The meteorological field for NAQPMS was provided by the Weather Research and Forecasting (WRF) model[32] (Text S1). The Double-Moment 6-class scheme (WDM6)[33] for microphysics scheme (MPS) was chosen in this study. The SST was not updated but only taken from FNL reanalysis data as the inputs for the WRF model. However, the updated or not values for SST were conducted in simulations of the sensitivity tests. The results for both precipitation and wet deposition were qualitatively similar (Figure S1). The simulations began at 0000 UTC on 20 July 2020 and ended at 0000 UTC on 8

Table 1. Statistics of Accumulated Precipitation and N_{ox} and N_{rd} Wet Depositions in Different Regions during Three Periods of Typhoon Hagupit and Comparison with Previous Studies[a]

Typhoon Hagupit		Prelandfall	Landfall			Postlandfall				Increment rate[b]	
		OU[b]	OU	YS[b]	EMC	YS	SJ[b]	EMC	KP	SJ[b]/OU[b]	YS[b]/OU[b]
N_{ox}	Mean (mg/m^2)	0.004	0.076	4.10	3.44	2.80	7.13	2.41	7.77	1782.5	1025.0
	Total amount (Mg)	5.78	56.52	1479.55	1715.79	1342.01	6877.51	963.11	1765.80	–	–
N_{rd}	Mean (mg/m^2)	0.005	0.06	4.86	6.26	1.66	2.31	11.52	4.84	462.0	972.0
	Total amount (Mg)	7.26	45.71	1756.61	3124.11	794.93	2225.43	4612.00	1100.58	–	–
N_r (N_{ox}+ N_{rd})	Mean (mm)	0.009	0.136	8.96	9.7	4.46	9.44	13.93	12.61	1048.9	995.6
	Total amount (Mg)	13.04	102.23	3236.16	4839.9	2136.94	9102.94	5575.11	2866.38	–	–
N_{ox}/N_{rd}	Mean	0.80	1.27	0.84	0.55	1.69	3.09	0.21	1.61	–	–
Pr	Mean (mm)	42.09	42.05	38.05	34.69	22.70	68.61	38.42	83.30	1.6	0.9
Area	(km^2)	1,321,517	746,148	361,211	499,081	479,105	964,433	400,428	227,381	–	–

Comparison of Nr wet deposition induced by typhoon with results from previous studies in each relevant region (unit: mgN m^{-2} day^{-1})

Region	Nitrogen species	Wet deposition during landfall and postlandfall[d]	Source and type[e]	Increment rate[c]
OU	HNO_3, NH_4^+, NH_3, NH_3^-, NO_x	0.0045	Ge et al.,[41] S	>10
OU	HNO_3, NH_4^+, NH_3, NH_3^-, NO_x	0.07	This study; S	–
YS	NH_3^-, NH_4^+	0.63	Itahashi et al.,[8] S	3.5–7.1
Qianliyan Island, YS	NHO_3, NH_4^+, NH_3, NH_3^-, NO_x	0.93	Zhang et al.,[5] O	2.4–4.8
YS	HNO_3, NH_4^+, NH_3, NH_3^-, NO_x	2.23–4.48	This study; S	–
SJ	NH_3^-, NH_4^+	0.52	Itahashi et al.,[9] S	9.1
SJ	HNO_3, NH_4^+, NH_3, NH_3^-, NO_x	4.72	This study, S	–
Eastern China	NH_4^-, NH_3^-, NO_x, NH_3	1.09–5.45	Zhang et al.,[5] S	–
EMC and KP	HNO_3, $NH_4^+NH_3$, NH_3^-, NO_x	4.85–6.3	This study, S	–

[a]Pr, precipitation; Nr, reactive nitrogen, including oxidized nitrogen (N_{ox}) and reduced nitrogen (N_{rd}); OU, ocean lying upwind of the Asian continent; YS, Yellow Sea, Bohai Sea, and part of the northern East China Sea; SJ, Sea of Japan; EMC, eastern mainland China; KP, Korean Peninsula. [b]Last two columns represent increment rates for N_{ox}, N_{rd}, N_r, and P_r over YS and SJ during landfall and postlandfall to corresponding variables over OU during prelandfall, respectively. [c]"Increment rate" columns represent increment rates for N_r wet deposition induced by the typhoon in our study to mean value in other studies, over OU, YS, and SJ, respectively. [d]Calculated from mean values divided by 2 days to transform to mgN m^{-2} day^{-1}. [e]S, simulation; O, observation.

August 2020, spanning the entire life cycle of typhoon Hagupit's passage over eastern China. Output from the first 10 days of the runs is not used in the subsequent discussions to allow sufficient time for model spin-up. Besides, another three typhoon cases (including Super Typhoon NEOGURI (2014) and VONGFONG (2014), which made landfall in Japan, and Typhoon MATMO (2014) swept through China) were conducted to enhance the reliability of the results. More detailed descriptions for the simulation as well as the eight sensitivity experiments for MPSs and SST can be found in SI Text S2.

Data and Typhoon Affected Regions. In this study, the model's output of N_r was classified as N_{ox} (including gaseous nitric acid (HNO_3), NO_x, and particulate NO_3^-; $N_{ox} = HNO_3 + NO_x + NO_3^-$) and N_{rd} (including gaseous NH_3 and particulate NH_4^+; $N_{rd} = NH_3 + NH_4^+$). The observational NO_3^- and NH_4^+ wet deposition data were collected from China National Environmental Monitoring Centre (CNEMC) and EANET (marked by triangles and squares in Figure 1a). To examine the typhoon-induced marine ecological response, chlorophyll-a (Chl-a) concentration associated with phytoplankton blooms was derived from the Copernicus Marine Environment Monitoring Service (CMEMS) Global Biogeochemical Analysis and Forecast (GBAF) product. Details of data source and processing method can be found in SI Text S3.

To quantity the typhoon-induced N wet deposition in more detail, we divided Hagupit's affected area into five regions representing the various geoclimatic regions of East Asia as shown in Figure 1a: (i) ocean upwind of the Asian continent (OU, including part of the southern East China Sea, the northeastern South China Sea, and the open ocean), (ii)YS, Bohai Sea, and part of the northern East China Sea, (iii) SJ, (iv) eastern mainland China (EMC), and (v) Korean Peninsula (KP). See SI Text S4 for details on the determination of typhoon-affected regions.

Typhoon Track and Model Validation. Hagupit formed as a tropical depression on 30 July in the Philippine Sea, then traveled northwestward and strengthened into a tropical storm later on the same day, and gradually intensified into a typhoon by 0900 UTC on 2 August. At 1930 UTC on 3 August, it was upgraded to a severe tropical storm and making landfall in Zhejiang, China, at peak intensity. After its landfall, Hagupit gradually weakened over China before degenerating into an extratropical cyclone on 6 August. In this study, Hagupit between 1 and 6 August 2020 (i.e., during Hagupit's passage over East Asia) was targeted, which were divided into the stages of prelandfall (before Hagupit's landfall, 1–2 August), landfall (during Hagupit's landfall, 3–4 August), and postlandfall (after re-emerging over the sea, 5–6 August).

The simulated surface precipitation captured the overall pattern represented in the observation from Global Precipitation Measurement-Integrated Multisatellite Retrieval (GPM-IMERG) (Text S3), albeit slightly overestimated over the land and underestimated over the ocean. In addition to precipitation, the simulated wet depositions of N_{ox} and N_{rd} during Hagupit's passage also show the broadly consistent evolution with observed Nr wet deposition. There are significant enhancements for both simulated and observed Nr wet depositions over EMC and SJ during landfall and postlandfall compared with that over OU during prelandfall with an almost similar magnitude of the increasing factors (see SI Text S5 for details on model validation). Similar performances were also found in the other three typhoon cases (Figure S8).

■ RESULTS AND DISCUSSION

Typhoon-Induced Wet Deposition of Nr. Figure 2a–f shows the spatial distributions of N_{ox} and N_{rd} wet depositions, with the bar charts giving key results during prelandfall, landfall, and postlandfall of the typhoon. Table 1 summarizes the corresponding statistical results. For the ocean of the OU region, wet depositions of N_{ox} and N_{rd} along Hagupit's passage were almost negligible, until the typhoon's interaction with air masses with high N_r emissions over land, as displayed in Figure 2a–f. Typhoon-induced changes of N_r wet deposition over ocean areas were more obvious than over land. By contrast, during landfall and postlandfall, the wet depositions of N_{ox} and N_{rd} were centered along Hagupit's passage. Specifically, because the typhoon's airstreams and surrounding circulation collected N_r pollutants from the East Asian continent (EMC, KP) and delivered them to the low-emission ocean areas (including SJ and YS; see SI Figure S9), these oceans received large amounts of wet N_{ox} and N_{rd} deposition along Hagupit's passage. Compared to YS, a higher N_r wet deposition was seen over SJ (Table 1; Figure 2a–f), and the accumulated N_r reached up to 91.9 mgN m^{-2} with the maximum N_{ox} increasing from 20.8 to 66.1 mgN m^{-2} and N_{rd} increasing from 10.4 to 25.7 mgN m^{-2} during the nontyphoon-affected period (3–4 August) to the typhoon-affected period (5–6 August). Besides, although the precipitation over OU virtually did not change from prelandfall to landfall (Table 1, ∼42 mm), the wet deposition of N_r over YS and SJ during landfall and postlandfall even reached up to 1000 times that over OU during prelandfall. Moreover, some other wet deposition results reported in the literature are compared with our simulation results. As shown in Table 1, the increment rates of typhoon-induced wet deposition in YS compared to the observed of Qianliyan Island by Zhang et al.[34] and simulated values by Itahashi et al.[8] are 2.4–4.8 and 3.5–7.1, respectively. The simulated wet N_r deposition of 4.72 mgN m^{-2} day^{-1} in SJ is 9 times the annual wet deposition (0.52 mgN m^{-2} day^{-1}) simulated by Itahashi et al.[8] (see SI Text S5 for more description).

Mechanisms of Nr Wet Deposition Induced by Landfalling Typhoon. The high Nr deposition during the typhoon's passage especially over the oceans was due to the "pumping effect" of the landfalling typhoon. As presented in the schematic diagram (Figure 1d), deep convective transports associated with cyclones are significant,[35,36] which uplifted the Nr emitted at ground level into the free troposphere[37,38] and were subsequently transported as well as deposited through the cyclone's counterclockwise motion to downwind areas.[35,39,20]

Based on NAQPMS, it is clarified that the strong uplifts of a typhoon can rapidly transport surface-layer N_{ox} up to higher heights (2–3 km) in less than 10 h, and N_{ox} could even be raised to 4 km when the typhoon makes landfall (SI Figure S10), which is remarkably higher than the normal vertical transport height of pollutants (0.6–0.8 km) driven by the boundary layer turbulent mixing mechanism.[40] This makes it easy for the pollutants to be captured by cloud droplets and long-range transported and hence deposited via the in-cloud scavenging process. The source apportionments for below-cloud and in-cloud Nr wet deposition in China, South Korea (SK), SJ, and Japan (JP), during postlandfall stages (5–6 August), were implemented in NAQPMS. As expected, the in-cloud scavenging process contributed 61% and 85% of the wet depositions in JP and SJ (Tables S2 and S3), respectively. This is also observed by Ge et al.,[41] who reported a larger contribution from the in-cloud scavenging process during strong vertical convection conditions in Beijing. The main contributions for N_{rd} in SJ (28.5%, 0.65 mg/m2) and the largest contributor 32.7% (0.93 mg/m2) to N_{ox} in JP were from the key landfall area of Hapupit, China, and SK via the in-cloud process, respectively. This implies that the significantly enhanced Nr wet deposition is not only the cause of the heavy precipitation, but also closely associated with the "pumping effect" of a typhoon. It should also be noted that the quantitative percentage of the source contributions was related to pollutant emissions and the intensity and path of the typhoon, as well as the uncertainties of the model simulations.

Marine Ecological Response. The typhoon-induced N_r deposition led to the activated biological process with significant enhancement in Chl-a concentration. The average Chl-a concentration associated with landfalling typhoon-induced phytoplankton blooms was around 0.44 mg m^{-3}, which was about 72% higher than the pretyphoon Chl-a levels (Figures 2g–i). Furthermore, the typhoon-induced wet deposition of N_r would then have created carbon fixation in the marine biological productivity of 12.67–25.44 mgC m^{-2} day^{-1} in YS and 26.8 mgC m^{-2} day^{-1} in SJ. At the same time, we have also studied the corresponding Chl-a concentration changes caused by the other three typhoons Neoguri, Vongfong, and Matmo from summer to autumn, as shown in Figure S11, which suggested that the typhoon-induced Nr deposition led to the activated biological process with significant enhancement in Chl-a concentration in spite of seasonal changes. The average Chl-a concentration associated with landfalling typhoon-induced phytoplankton blooms was around 0.50–0.65 mg m^{-3}, which was about 32%–73% higher than the pretyphoon Chl-a levels. These results are a further indication that human activities could greatly influence the marine ecosystem through typhoon-induced atmospheric input.[5] As a consequence, anthropogenic emissions especially in coastal cities should be considered more carefully to safeguard the marine ecosystem.

Future Prospect. The above results demonstrate the importance of accurately quantifying how anthropogenic activities influence the ocean ecosystem when typhoons occur. Meanwhile, the frequency of landfalling cyclones has increased substantially in the last few decades. This has resulted from cyclone poleward migration, principally because of the change in the large-scale steering flow and warmer relative sea surface temperature along the coast of China.[42,43] As the world continues to warm, cyclones will extend progressively farther inland, with intensification and slower decay of landfalling cyclones.[44] Additional studies should be conducted to investigate the "pumping effect" in other areas. Also, the uncertainties in Nr wet deposition simulations such as meteorological fields, typhoon intensities, and emissions of pollutants are very worthwhile issues to discuss and deserve further research in the future.

■ ASSOCIATED CONTENT

Supporting Information

The Supporting Information is available free of charge at https://pubs.acs.org/doi/10.1021/acs.estlett.2c00762.

https://doi.org/10.1021/acs.estlett.2c00762
Environ. Sci. Technol. Lett. 2022, 9, 1014–1021

Detailed descriptions about NAQPMS and WRF configurations, typhoon-affected areas, sensitivity experiments, Nr wet deposition measurements (CNEMC and EANET), biogeochemical reanalysis data (CMEMS-GBAF) and the processing method, satellite precipitation data (GPM-IMERG), model validations, three other landing typhoon events, and supporting tables figures (PDF)

■ AUTHOR INFORMATION

Corresponding Author

Baozhu Ge − *State Key Laboratory of Atmospheric Boundary Layer Physics and Atmospheric Chemistry, Institute of Atmospheric Physics, Chinese Academy of Sciences, Beijing 100029, China;* orcid.org/0000-0002-6763-7730; Email: gebz@mail.iap.ac.cn

Authors

Ying Zhang − *State Key Laboratory of Atmospheric Boundary Layer Physics and Atmospheric Chemistry, Institute of Atmospheric Physics, Chinese Academy of Sciences, Beijing 100029, China;* orcid.org/0000-0003-4968-8144

Xingtao Su − *Beijing Institute of Applied Meteorology, Beijing 100029, China*

Xiaobin Xu − *Key Laboratory for Atmospheric Chemistry, Chinese Academy of Meteorological Sciences, Beijing 100081, China;* orcid.org/0000-0003-4321-9267

Qixin Tan − *State Key Laboratory of Atmospheric Boundary Layer Physics and Atmospheric Chemistry, Institute of Atmospheric Physics, Chinese Academy of Sciences, Beijing 100029, China; University of Chinese Academy of Sciences, Beijing 100049, China*

Guanghua Chen − *State Key Laboratory of Atmospheric Boundary Layer Physics and Atmospheric Chemistry, Institute of Atmospheric Physics, Chinese Academy of Sciences, Beijing 100029, China*

Danhui Xu − *National Center for Climate Change Strategy and International Cooperation, Ministry of Ecology and Environment, Beijing 100035, China*

Xueshun Chen − *State Key Laboratory of Atmospheric Boundary Layer Physics and Atmospheric Chemistry, Institute of Atmospheric Physics, Chinese Academy of Sciences, Beijing 100029, China*

Lin Wu − *State Key Laboratory of Atmospheric Boundary Layer Physics and Atmospheric Chemistry, Institute of Atmospheric Physics, Chinese Academy of Sciences, Beijing 100029, China*

Meng Gao − *Department of Geography, Hong Kong Baptist University, Hong Kong SAR 999077, China;* orcid.org/0000-0002-8657-3541

Xiaole Pan − *State Key Laboratory of Atmospheric Boundary Layer Physics and Atmospheric Chemistry, Institute of Atmospheric Physics, Chinese Academy of Sciences, Beijing 100029, China*

Jianping Guo − *State Key Laboratory of Severe Weather, Chinese Academy of Meteorological Sciences, Beijing 100081, China;* orcid.org/0000-0001-8530-8976

Xuejun Liu − *College of Resources and Environmental Sciences, China Agricultural University, Beijing 100193, China;* orcid.org/0000-0002-8367-5833

Joshua S. Fu − *Department of Civil and Environmental Engineering, University of Tennessee, Knoxville, Tennessee 37996, United States;* orcid.org/0000-0001-5464-9225

Zifa Wang − *State Key Laboratory of Atmospheric Boundary Layer Physics and Atmospheric Chemistry, Institute of Atmospheric Physics, Chinese Academy of Sciences, Beijing 100029, China; University of Chinese Academy of Sciences, Beijing 100049, China*

Complete contact information is available at: https://pubs.acs.org/10.1021/acs.estlett.2c00762

Notes

The authors declare no competing financial interest.

■ ACKNOWLEDGMENTS

We appreciate Dr. Syuichi Itahashi from CRIEPI, JAPAN and EANET for providing the observation data. This work was financially supported by the National Science Foundation of China (Grants 41877313 and 42122049), and the Strategic Priority Research Program (A) of the Chinese Academy of Sciences (Grant XDA19040204), and the National Key Scientific and Technological Infrastructure project "Earth System Science Numerical Simulator Facility" (EarthLab).

■ REFERENCES

(1) Krishnamurthy, A.; Moore, J. K.; Zender, C. S.; Luo, C. Effects of atmospheric inorganic nitrogen deposition on ocean biogeochemistry. *J. Geophys. Res. Biogeo.* **2007**, *112* (G2), na DOI: 10.1029/2006JG000334.

(2) Duce, R. A.; LaRoche, J.; Altieri, K.; Arrigo, K. R.; Baker, A. R.; Capone, D. G.; Cornell, S.; Dentener, F.; Galloway, J.; Ganeshram, R. S.; Geider, R. J.; Jickells, T.; Kuypers, M. M.; Langlois, R.; Liss, P. S.; Liu, S. M.; Middelburg, J. J.; Moore, C. M.; Nickovic, S.; Oschlies, A.; Pedersen, T.; Prospero, J.; Schlitzer, R.; Seitzinger, S.; Sorensen, L. L.; Uematsu, M.; Ulloa, O.; Voss, M.; Ward, B.; Zamora, L. Impacts of atmospheric anthropogenic nitrogen on the open ocean. *Science* **2008**, *320* (5878), 893−897.

(3) Doney, S. C.; Mahowald, N.; Lima, I.; Feely, R. A.; Mackenzie, F. T.; Lamarque, J.-F.; Rasch, P. J. Impact of anthropogenic atmospheric nitrogen and sulfur deposition on ocean acidification and the inorganic carbon system. *Proc. Natl. Acad. Sci. U.S.A.* **2007**, *104* (37), 14580−14585.

(4) Suntharalingam, P.; Buitenhuis, E.; Le Quere, C.; Dentener, F.; Nevison, C.; Butler, J. H.; Bange, H. W.; Forster, G. Quantifying the impact of anthropogenic nitrogen deposition on oceanic nitrous oxide. *Geophys. Res. Lett.* **2012**, *39*, na.

(5) Zhang, Y.; Yu, Q.; Ma, W.; Chen, L. Atmospheric deposition of inorganic nitrogen to the eastern China seas and its implications to marine biogeochemistry. *J. Geophys. Res. Atmos.* **2010**, *115*, na DOI: 10.1029/2009JD012814.

(6) Zhang, J.; Liu, M. G. Observations on nutrient elements and sulphate in atmospheric wet depositions over the northwest Pacific coastal oceans - Yellow Sea. *Mar. Chem.* **1994**, *47* (2), 173−189.

(7) Zhang, J.; Liu, S. M.; Ren, J. L.; Wu, Y.; Zhang, G. L. Nutrient gradients from the eutrophic Changjiang (Yangtze River) Estuary to the oligotrophic Kuroshio waters and re-evaluation of budgets for the East China Sea Shelf. *Prog. Oceanogr.* **2007**, *74* (4), 449−478.

(8) Itahashi, S.; Hayashi, K.; Takeda, S.; Umezawa, Y.; Matsuda, K.; Sakurai, T.; Uno, I. Nitrogen burden from atmospheric deposition in East Asian oceans in 2010 based on high-resolution regional numerical modeling. *Environ. Pollut.* **2021**, *286*, 117309.

(9) Liu, X.; Duan, L.; Mo, J.; Du, E.; Shen, J.; Lu, X.; Zhang, Y.; Zhou, X.; He, C.; Zhang, F. Nitrogen deposition and its ecological impact in China: An overview. *Environ. Pollut.* **2011**, *159* (10), 2251−2264.

(10) Kurokawa, J.; Ohara, T.; Morikawa, T.; Hanayama, S.; Janssens-Maenhout, G.; Fukui, T.; Kawashima, K.; Akimoto, H. Emissions of air pollutants and greenhouse gases over Asian regions during 2000−

2008: Regional Emission inventory in ASia (REAS) version 2. *Atmos. Chem. Phys.* **2013**, *13* (21), 11019−11058.
(11) Zhai, S.; Jacob, D. J.; Wang, X.; Liu, Z.; Wen, T.; Shah, V.; Li, K.; Moch, J. M.; Bates, K. H.; Song, S.; Shen, L.; Zhang, Y.; Luo, G.; Yu, F.; Sun, Y.; Wang, L.; Qi, M.; Tao, J.; Gui, K.; Xu, H.; Zhang, Q.; Zhao, T.; Wang, Y.; Lee, H. C.; Choi, H.; Liao, H. Control of particulate nitrate air pollution in China. *Nat. Geosci.* **2021**, *14* (6), 389.
(12) Kuttippurath, J.; Singh, A.; Dash, S. P.; Mallick, N.; Clerbaux, C.; Van Damme, M.; Clarisse, L.; Coheur, P. F.; Raj, S.; Abbhishek, K.; Varikoden, H. Record high levels of atmospheric ammonia over India: Spatial and temporal analyses. *Sci. Total Environ.* **2020**, *740*, 139986.
(13) Van Damme, M.; Clarisse, L.; Franco, B.; Sutton, M. A.; Erisman, J. W.; Wichink Kruit, R.; van Zanten, M.; Whitburn, S.; Hadji-Lazaro, J.; Hurtmans, D.; Clerbaux, C.; Coheur, P.-F. Global, regional and national trends of atmospheric ammonia derived from a decadal (2008−2018) satellite record. *Environ. Res. Lett.* **2021**, *16* (5), 055017.
(14) Lachatre, M.; Fortems-Cheiney, A.; Foret, G.; Siour, G.; Dufour, G.; Clarisse, L.; Clerbaux, C.; Coheur, P.-F.; Van Damme, M.; Beekmann, M. The unintended consequence of SO_2 and NO_2 regulations over China: increase of ammonia levels and impact on $PM_{2.5}$ concentrations. *Atmos. Chem. Phys.* **2019**, *19* (10), 6701−6716.
(15) Fu, X.; Wang, S.; Xing, J.; Zhang, X.; Wang, T.; Hao, J. Increasing Ammonia Concentrations Reduce the Effectiveness of Particle Pollution Control Achieved via SO_2 and NO_X Emissions Reduction in East China. *Environ. Sci. Technol. Lett.* **2017**, *4* (6), 221−227.
(16) Itahashi, S.; Yumimoto, K.; Uno, I.; Hayami, H.; Fujita, S.-i.; Pan, Y.; Wang, Y. A 15-year record (2001−2015) of the ratio of nitrate to non-sea-salt sulfate in precipitation over East Asia. *Atmos. Chem. Phys.* **2018**, *18* (4), 2835−2852.
(17) Moon, J.-Y.; Lee, K.; Lim, W.-A.; Lee, E.; Dai, M.; Choi, Y.-H.; Han, I.-S.; Shin, K.; Kim, J.-M.; Chae, J. Anthropogenic nitrogen is changing the East China and Yellow seas from being N deficient to being P deficient. *Limnol. Oceanogr.* **2021**, *66* (3), 914−924.
(18) Ge, B.; Itahashi, S.; Sato, K.; Xu, D.; Wang, J.; Fan, F.; Tan, Q.; Fu, J. S.; Wang, X.; Yamaji, K.; Nagashima, T.; Li, J.; Kajino, M.; Liao, H.; Zhang, M.; Wang, Z.; Li, M.; Woo, J.-H.; Kurokawa, J.; Pan, Y.; Wu, Q.; Liu, X.; Wang, Z. Model Inter-Comparison Study for Asia (MICS-Asia) phase III: multimodel comparison of reactive nitrogen deposition over China. *Atmos. Chem. Phys.* **2020**, *20* (17), 10587−10610.
(19) Zhang, J.; Guo, X.; Zhao, L. Tracing external sources of nutrients in the East China Sea and evaluating their contributions to primary production. *Prog. Oceanogr.* **2019**, *176*, 102122.
(20) Felix, J. D.; Murgulet, D. Nitrate isotopic composition of sequential Hurricane Harvey wet deposition: Low latitude NOx sources and oxidation chemistry. *Atmos. Environ.* **2020**, *238*, 117748.
(21) Miller, C.; Willey, J. D.; Kieber, R. J. Changes in rainwater composition in Wilmington, NC during tropical storm Ernesto. *Atmos. Environ.* **2008**, *42* (5), 846−855.
(22) Clark, C. M.; Phelan, J.; Doraiswamy, P.; Buckley, J.; Cajka, J. C.; Dennis, R. L.; Lynch, J.; Nolte, C. G.; Spero, T. L. Atmospheric deposition and exceedances of critical loads from 1800−2025 for the conterminous United States. *Ecol. Appl.* **2018**, *28* (4), 978−1002.
(23) Kuttippurath, J.; Sunanda, N.; Martin, M. V.; Chakraborty, K. Tropical storms trigger phytoplankton blooms in the deserts of north Indian Ocean. *npj Clim. Atmos. Sci.* **2021**, *4* (1), na DOI: 10.1038/s41612-021-00166-x.
(24) Yang, J. Y. T.; Hsu, S. C.; Dai, M. H.; Hsiao, S. S. Y.; Kao, S. J. Isotopic composition of water-soluble nitrate in bulk atmospheric deposition at Dongsha Island: sources and implications of external N supply to the northern South China Sea. *Biogeosciences* **2014**, *11* (7), 1833−1846.
(25) Wang, Z. F.; Maeda, T.; Hayashi, M.; Hsiao, L. F.; Liu, K. Y. A nested air quality prediction modeling system for urban and regional scales: Application for high-ozone episode in Taiwan. *Water Air Soil Poll.* **2001**, *130* (1−4), 391−396.
(26) Li, J.; Yang, W.; Wang, Z.; Chen, H.; Hu, B.; Li, J.; Sun, Y.; Fu, P.; Zhang, Y. Modeling study of surface ozone source-receptor relationships in East Asia. *Atmos. Res.* **2016**, *167*, 77−88.
(27) Wang, Z.; Pan, X.; Uno, I.; Li, J.; Wang, Z.; Chen, X.; Fu, P.; Yang, T.; Kobayashi, H.; Shimizu, A.; Sugimoto, N.; Yamamoto, S. Significant impacts of heterogeneous reactions on the chemical composition and mixing state of dust particles: A case study during dust events over northern China. *Atmos. Environ.* **2017**, *159*, 83−91.
(28) Ge, B. Z.; Wang, Z. F.; Xu, X. B.; Wu, J. B.; Yu, X. L.; Li, J. Wet deposition of acidifying substances in different regions of China and the rest of East Asia: Modeling with updated NAQPMS. *Environ. Pollut.* **2014**, *187*, 10−21.
(29) Li, M.; Zhang, Q.; Kurokawa, J. I.; Woo, J. H.; He, K.; Lu, Z.; Ohara, T.; Song, Y.; Streets, D. G.; Carmichael, G. R.; Cheng, Y.; Hong, C.; Huo, H.; Jiang, X.; Kang, S.; Liu, F.; Su, H.; Zheng, B. MIX: a mosaic Asian anthropogenic emission inventory under the international collaboration framework of the MICS-Asia and HTAP. *Atmos. Chem. Phys.* **2017**, *17* (2), 935−963.
(30) Guenther, A.; Karl, T.; Harley, P.; Wiedinmyer, C.; Palmer, P. I.; Geron, C. Estimates of global terrestrial isoprene emissions using MEGAN (Model of Emissions of Gases and Aerosols from Nature). *Atmos. Chem. Phys.* **2006**, *6* (11), 3181−3210.
(31) van der Werf, G. R.; Randerson, J. T.; Giglio, L.; Collatz, G. J.; Mu, M.; Kasibhatla, P. S.; Morton, D. C.; DeFries, R. S.; Jin, Y.; van Leeuwen, T. T. Global fire emissions and the contribution of deforestation, savanna, forest, agricultural, and peat fires (1997−2009). *Atmos. Chem. Phys.* **2010**, *10* (23), 11707−11735.
(32) Skamarock, W. C.; Klemp, J. B.; Dudhia, J.; Gill, D. O.; Barker, D.; Duda, M. G.; Huang, X.; Wang, W.; Powers, J. G. *A Description of the Advanced Research WRF Version 3*; No. NCAR/TN-475+STR; University Corporation for Atmospheric Research, 2008. DOI: 10.5065/D68S4MVH.
(33) Hong, S.-Y.; Lim, K.-S. S.; Lee, Y.-H.; Ha, J.-C.; Kim, H.-W.; Ham, S.-J.; Dudhia, J. Evaluation of the WRF Double-Moment 6-Class Microphysics Scheme for Precipitating Convection. *Adv. Meteorol.* **2010**, *2010*, 1.
(34) Zhang, G.; Zhang, J.; Liu, S. Characterization of nutrients in the atmospheric wet and dry deposition observed at the two monitoring sites over Yellow Sea and East China Sea. *J. Geophys. Res. Atmos.* **2007**, *57* (1), 41−57.
(35) Cao, H.; Henze, D. K.; Cady-Pereira, K.; McDonald, B. C.; Harkins, C.; Sun, K.; Bowman, K. W.; Fu, T.-M.; Nawaz, M. O. COVID-19 Lockdowns Afford the First Satellite-Based Confirmation That Vehicles Are an Under-recognized Source of Urban NH3 Pollution in Los Angeles. *Environ. Sci. Technol. Lett.* **2022**, *9* (1), 3−9.
(36) Miyazaki, Y.; Kondo, Y.; Koike, M.; Fuelberg, H. E.; Kiley, C. M.; Kita, K.; Takegawa, N.; Sachse, G. W.; Flocke, F.; Weinheimer, A. J.; Singh, H. B.; Eisele, F. L.; Zondlo, M.; Talbot, R. W.; Sandholm, S. T.; Avery, M. A.; Blake, D. R. Synoptic-scale transport of reactive nitrogen over the western Pacific in spring. *J. Geophys. Res. Atmos.* **2003**, *108* (D20), na DOI: 10.1029/2002JD003248.
(37) Fadnavis, S.; Beig, G.; Buchunde, P.; Ghude, S. D.; Krishnamurti, T. N. Vertical transport of ozone and CO during super cyclones in the Bay of Bengal as detected by Tropospheric Emission Spectrometer. *Environ. Sci. Pollut.* **2011**, *18* (2), 301−315.
(38) Bethan, S.; Vaughan, G.; Gerbig, C.; Volz-Thomas, A.; Richer, H.; Tiddeman, D. A. Chemical air mass differences near fronts. *J. Geophys. Res. Atmos.* **1998**, *103* (D11), 13413−13434.
(39) Kiley, C. M.; Fuelberg, H. E. An examination of summertime cyclone transport processes during intercontinental chemical transport experiment (INTEX-A). *J. Geophys. Res. Atmos.* **2006**, *111* (D24), na DOI: 10.1029/2006JD007115.
(40) Shi, D.; Chen, G. The Implication of Outflow Structure for the Rapid Intensification of Tropical Cyclones under Vertical Wind Shear. *Mon. Weather Rev.* **2021**, *149* (12), 4107−4127.
(41) Ge, B.; Xu, D.; Wild, O.; Yao, X.; Wang, J.; Chen, X.; Tan, Q.; Pan, X.; Wang, Z. Inter-annual variations of wet deposition in Beijing

from 2014–2017: implications of below-cloud scavenging of inorganic aerosols. *Atmos. Chem. Phys.* **2021**, *21* (12), 9441–9454.

(42) Kang, H.; Zhu, B.; Gao, J.; He, Y.; Wang, H.; Su, J.; Pan, C.; Zhu, T.; Yu, B. Potential impacts of cold frontal passage on air quality over the Yangtze River Delta, China. *Atmos. Chem. Phys.* **2019**, *19* (6), 3673–3685.

(43) Sun, J.; Wang, D.; Hu, X.; Ling, Z.; Wang, L. Ongoing Poleward Migration of Tropical Cyclone Occurrence Over the Western North Pacific Ocean. *Geophys. Res. Lett.* **2019**, *46* (15), 9110–9117.

(44) Song, J.; Klotzbach, P. J.; Zhao, H.; Duan, Y. Slowdown in the Decay of Western North Pacific Tropical Cyclones Making Landfall on the Asian Continent. *Front. Earth Sci.* **2021**, *9*, na DOI: 10.3389/feart.2021.749287.

https://doi.org/10.1021/acs.estlett.2c00762
Environ. Sci. Technol. Lett. 2022, 9, 1014–1021